

27 an experimental setup would allow to research the interaction of highly rarefied, ionized gas
28 flows with satellite components and structures. The pumping capabilities of the facility allow
29 the testing of electric propulsion, which has been its main purpose so far but also becomes
30 interesting within the context of ABEP. A special focus shall be put on the possibility to conduct
31 long-term test campaigns within the scope of weeks or months within the facility, which has
32 been proven successfully within previous experimental campaigns for the industry. Therefore,
33 the qualification of systems for the VLEO environment seems feasible within the STG-ET
34 facility. Further activities and facilities at the DLR Göttingen related to electric propulsion and
35 rarefied gas flows will be discussed.

36

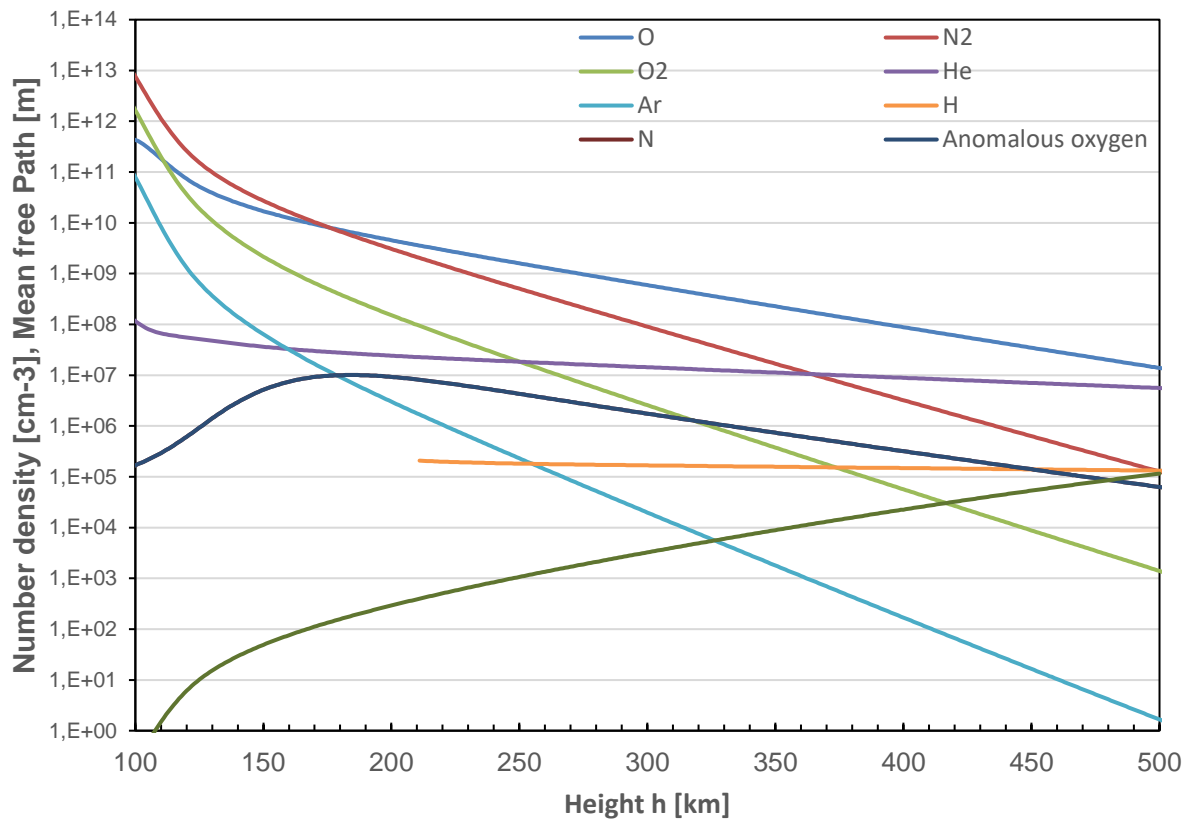
37 **1. Introduction**

38 With the growing interest for missions within the very low-earth-orbit (VLEO), especially for
39 earth observation and communications [1], the advancement of understanding of the interaction
40 of the spacecraft with the residual atmosphere becomes necessary. The applications of interest
41 are e.g. aerodynamic maneuvers for satellites [2], in situ resource utilization for air-breathing
42 electric propulsion (ABEP) [3] as well as aerocapture or aerobraking for re-entry missions [4].
43 These missions are often planned to operate for years, making the qualification of the equipment
44 necessary. In addition, the mission analysis and design require experimental data to verify
45 numerical results [5]. While (thermal) vacuum chambers to reproduce the space environment
46 in low-earth-orbit (LEO) or for geostationary orbits (GEO) are quite common, facilities which
47 reproduce the conditions in the VLEO, especially the high-velocity flow ($v_\infty \approx 8$ km/s) of the
48 neutral atoms of the residual atmosphere are quite rare[6]–[9]. With the increase of demand for
49 such facilities, it becomes therefore necessary to establish or upgrade more ‘wind tunnels’
50 capable of recreating such an environment. The main challenges are here the pumping
51 capabilities for gas flows within the chamber as well as the acceleration of flows to the free-
52 stream velocity observed in LEO. This work shall demonstrate some of the capabilities of the
53 vacuum wind tunnels and chambers at the Institute of Aerodynamics and Flow Technology at
54 the DLR Göttingen and modifications or extensions necessary to study high velocity, low
55 density flows as they occur in the VLEO. While there are multiple facilities available, some of
56 which have up to 50 years of operational experience [Ref VXG], this work will focus mainly
57 on the STG-ET facility, which has been built 10 years ago with a special focus on long-duration
58 test campaigns for the qualification of electric propulsion [Ref STGET]. Since the vacuum
59 systems of this facility is designed to resemble the space environment, the atmospheric
60 conditions in terms of pressure and density of the LEO are well within their operational range.
61 Still, the creation of a low-density, high velocity flow of neutrals is very challenging, therefore

62 different methods of flow creation and their possible implementation will be discussed. The
63 design methods for the VxG facility, which has been built in the 1970s to study low-density
64 hypersonic flows using the molecular beam technique, will be implemented for the STG-ET
65 facility. Finally, the feasibility of the STG-ET facility for the simulation of atmospheric flows
66 will be evaluated and possible upgrades will be described.

67 **2. Conditions in the VLEO**

68 The very-low-earth-orbit (VLEO) is used as a term to describe an orbit in between heights of
69 200 km to 450 km above the ground [1], which offers advantages for earth-observation
70 missions. Within the VLEO, flow conditions are dominated by the residual atmosphere, mostly
71 consisting of atomic oxygen. The number densities n of the most important species within the
72 residual atmosphere are displayed in Fig. REF as a function of height according to the empirical
73 NRLMSISE-00 model [10]. It can be seen, that between 200 km and 450 km besides molecular
74 oxygen (O₂) and nitrogen (N₂), atomic oxygen (O) becomes the most dominant species.
75 Additionally, the temperature, pressure, density, mean free path and Mach number are displayed
76 in Fig REF2. To calculate the Mach number, the velocity is assumed to be the orbital velocity
77 neglecting the drag forces of the residual atmosphere, resulting in a free stream velocity of
78 $v_\infty \approx 8$ km/s. Additionally, the Knudsen number has been calculated with a reference length
79 of $L = 1$ m. It can be seen, that depending on height, a free molecular flow cannot be assumed
80 and a transitional regime or slip-flow is more likely to occur, especially for larger spacecraft.



81

82 *Figure 1: Number Density of molecular oxygen (O₂) and nitrogen (N₂), atomic oxygen (O) and*
 83 *nitrogen (N) and helium (He), argon (Ar) and hydrogen (H) as well as anomalous oxygen*
 84 *according to the NRLMSISE-00 model as a function of height above ground. Mean free path of*
 85 *air using the total number density as a function of height.*

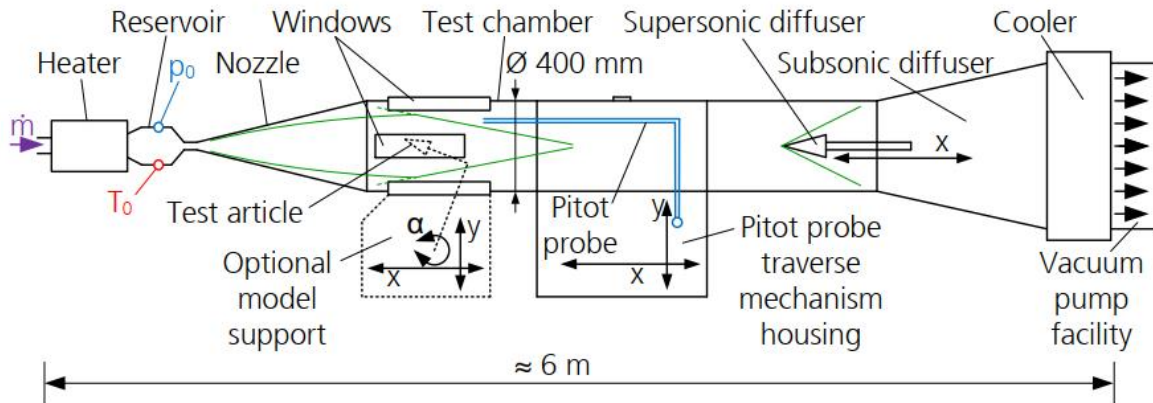
86 3. Vacuum chambers and wind tunnels at DLR Göttingen

87 The simulation of rarefied flows has a long history at the DLR in Göttingen, therefore multiple
88 vacuum chambers and wind tunnels are available which can produce the necessary low
89 pressures and densities to recreate environments similar to the atmosphere at high altitudes or
90 space. The different facilities are listed with references in Tab REF. Since these vacuum
91 chambers are used for the testing of propulsion, they are not capable of producing the necessary
92 flow conditions on their own. In the 1970s, the vacuum wind tunnels V1G, V2G [11], [12] and
93 V3G [11], [13] ('Vakuumwindkanal Göttingen') were used to study the aerodynamics of
94 satellites within hypersonic rarefied flows. Since the V1G vacuum wind tunnel has been
95 dismantled, only the V2G and V3G shall be briefly described, while further information can be
96 gained from the descriptions by Koppenwallner [11] and Wuest et al. [12].

97 *Table 1: List of Vacuum Wind Tunnels and Vacuum chambers available at DLR Göttingen*

Chamber	Type	Pressure [mbar]	Dimensions (LxD)	Mean Free Path of Air molecules [m]
V2G [11]	Vacuum Wind Tunnel	1E-3	6x0.4m	0.0094
V3G [11]	Vacuum Wind Tunnel	1.5E-8	2.5x1.25m	0.008
STG-MT	Propulsion Test	3E-6	2x1m	3.14
STG-ET [11],[12]	Propulsion Test	4E-7	12.2x5m	23.5
STG-CT [16]	Propulsion Test	1E-10	6.25x1.6m	1200

98



99

100

Figure 2: Picture and diagram of the V2G Vacuum Wind Tunnel [17]

101

Within a hypersonic vacuum wind tunnel such as the V2G and V3G available at the DLR, high

102

Mach number flows are created by the expansion of a gas due to a large pressure difference

103

between the vacuum background pressure and the reservoir pressure. Due to the decrease in

104

temperature of an expanding gas, for a very high flow velocity, the gas also needs to be heated

105

within the reservoir to avoid condensation within the nozzle, which can be done either by an

106

graphite heater as used in the V2G wind tunnel (displayed in Figure 2) or the use of an inductive

107

plasma heater initially used at the V3G [18]. Since the heating of the gas is sometimes not

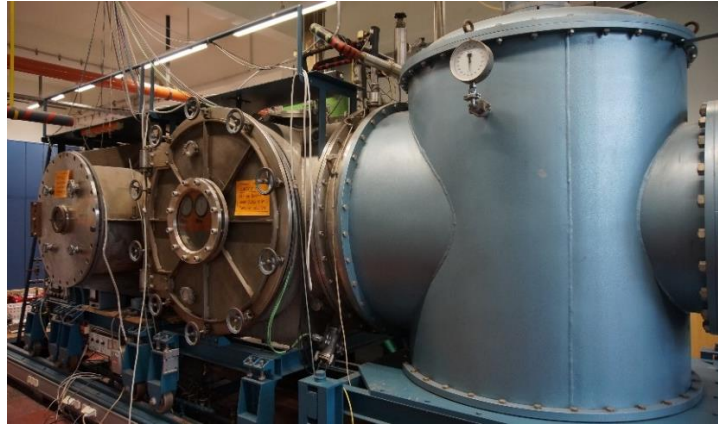
108

desired and this technique also does not avoid the formation of a large boundary layer, another

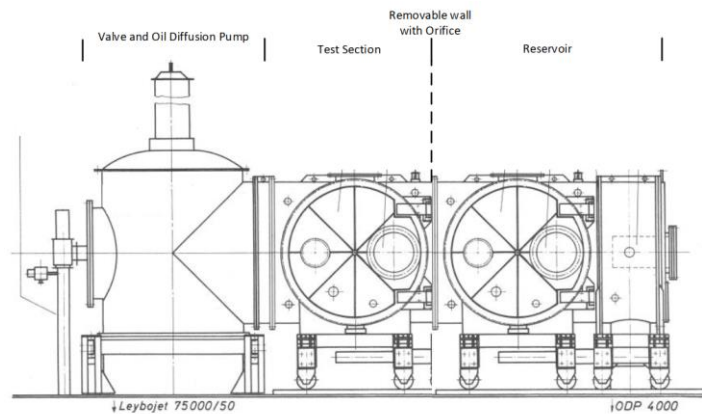
109

technique to create the desired flows can be used.

110



111



112

Figure 3: Picture and diagram of the V3G Vacuum Wind Tunnel

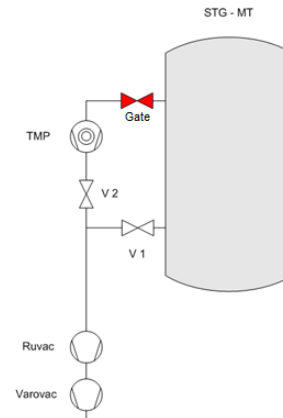
113 At the V3G facility, as shown in Figure 3, the vacuum chamber of the wind tunnel is separated
114 in 2 segments, with a test section and a reservoir separated by a skimmer and collimator. The
115 resulting Knudsen effusion through an orifice is then sufficient to create a molecular free stream
116 with the desired velocities and densities and a very homogenous velocity distribution within the
117 molecular jet with a Mach number $Ma = 7$ at a mean free path of around $\lambda = 8$ mm. The
118 pumping system of the facility consists of multiple roughing pumps, while the final vacuum
119 pressure can be reached using two oil diffusion pumps, one installed in the test section and one in
120 the reservoir section. In addition, the chamber walls can be cooled by using liquid nitrogen,
121 giving additional cryogenic pumping capacity.



122

123 *Figure 4: The STG-CT facility with door open and view onto helium cryo pump*

124 For the testing of chemical propulsion, the STG-CT [16] (“Simulationsanlage für Treibstrahlen
125 Göttingen – Chemische Triebwerke”) facility is used, which is designed for extremely low
126 pressures. This is established using a liquid helium-driven cryopump with an area of about 30m³
127 which encloses the test section, maintaining a wall temperature of 4.2 K. This inner cryopump,
128 as seen in Figure 4, is completely enclosed by a liquid nitrogen cooled surface, enclosed by the
129 vacuum chamber, which is evacuated using a set of Leybold roots and rotary vane roughing
130 pumps and a turbomolecular pump. With this setup, pressures of up to 10⁻¹⁰ mbar can be
131 reached, even with hydrogen still standby pressures as low as 10⁻⁵ mbar can be reached,
132 making this facility ideal for the research of plume interaction in space.



133

134

Figure 5: Picture and diagram of the STG-MT vacuum chamber

135

The smaller STG-MT chamber, shown in *Figure 5*, was used for the testing of chemical cold gas thrusters and is now used for testing of diagnostics for electric propulsion as well as to study sputtering of materials by electric thrusters [19]. The facility consists of a combined Leybold rotary vane and Roots pump and a Pfeiffer rurbomolecular pump, making it only viable for higher pressures and low gas flows.

139

140 **4. The STG-ET Facility**

141

Within this section the capabilities of the STG-ET facility, which has been built specifically for the simulation of a space environment, will be described [14], [15]. The facility, shown in *Figure 5* and schematically in *Figure 6* respectively consists of a vacuum tank with an inner diameter of 5 m and a length of 12.2 m. To create a rough vacuum, a set of two connected Pfeiffer vacuum pumps is used, which can sustain a base pressure of 10^{-2} mbar. Fine vacuum is created using 4 Edwards turbomolecular pumps connected to a second, smaller set of Pfeiffer roughing pumps, reaching a stand-by pressure of 10^{-6} mbar. The pressure can be lowered further by the use of 18 Oerlikon Leybold cryopumps reaching a stand-by pressure of $4 \cdot 10^{-7}$ mbar. With a gas flow into the facility, the nominal pressure is higher, as shown in *Figure 8* which displays the vacuum base pressure as a function of cold gas flow rate for argon, krypton

149

150

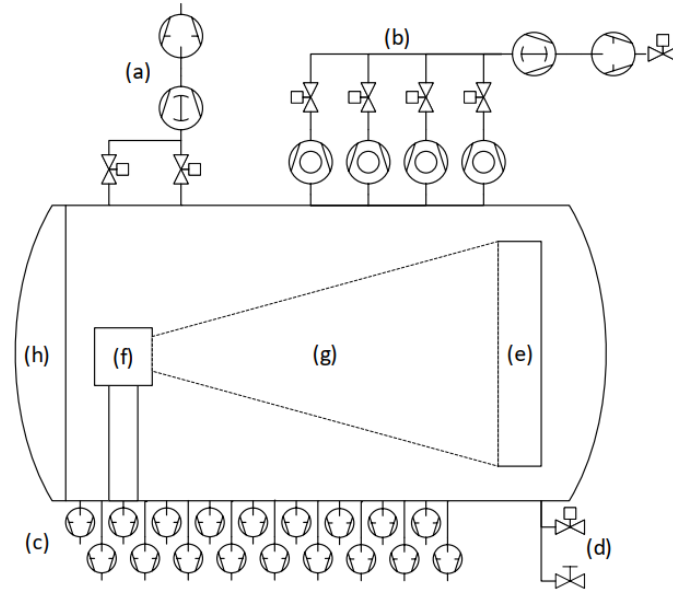
151 and xenon at room temperature [20]. The pumping speeds are $S(Xe) = 276000 \frac{l}{s}$ for xenon,
152 $S(Kr) = 360000 \frac{l}{s}$ for krypton and $S(Ar) = 452000 l/s$ for argon. Multiple diagnostics are
153 available within the facility. These are different robotic arms to support the installation of
154 plasma diagnostics for ion beams, a C-shaped set of Faraday cups to measure the beam current
155 from electric propulsion as well as thrust stands for propulsion. The gas composition can be
156 analyzed using a mass spectrometer. A large number of vacuum feedthroughs allows the simple
157 installation of additional diagnostics to support experiments and the use of optical measurement
158 methods through multiple windows. To shield the chamber walls from sputtering due to
159 energetic ions from propulsion, a water-cooled graphite target is installed at the rear end of the
160 chamber and the chamber walls are protected using graphite plates. As displayed in Figure 6
161 the whole lid of the chamber can be removed allowing easy access and installation of thrusters.
162 The vacuum chamber can operate continuously at low pressures for extended periods of time
163 up to several weeks or months, giving a unique opportunity for long-duration testing of electric
164 thrusters.



165

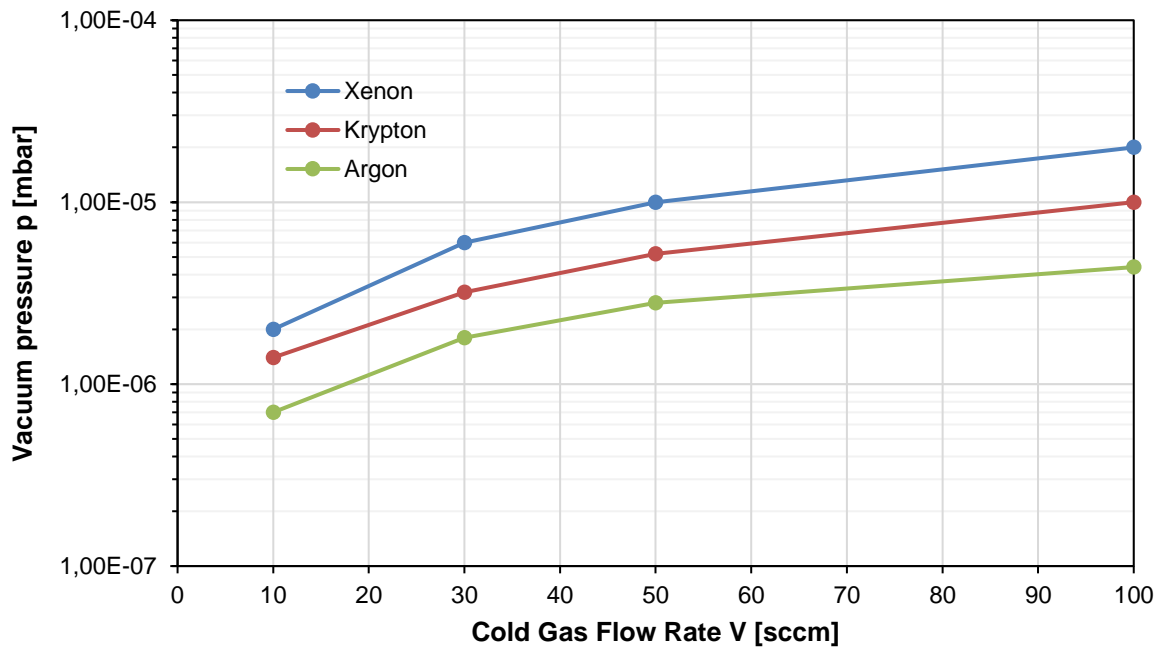
166

Figure 6: Picture of the opened STG-ET vacuum chamber



167

168 *Figure 7: Schematic of the STG-ET facility's vacuum system with (a) Roughing pumps (b)*
 169 *Turbomolecular pumps (c) Cryopumps (d) Venting valve (e) Beam Target (f) Plasma Source /*
 170 *Thruster on Diagnostics Tower (g) Plasma Beam (h) Chamber cover*



171

172 *Figure 8: Vacuum pressure of the STG-ET facility as a function of cold gas flow rate for*
 173 *different noble gases [20]*

174 **5. Feasibility of the STG-ET facility to simulate VLEO conditions**

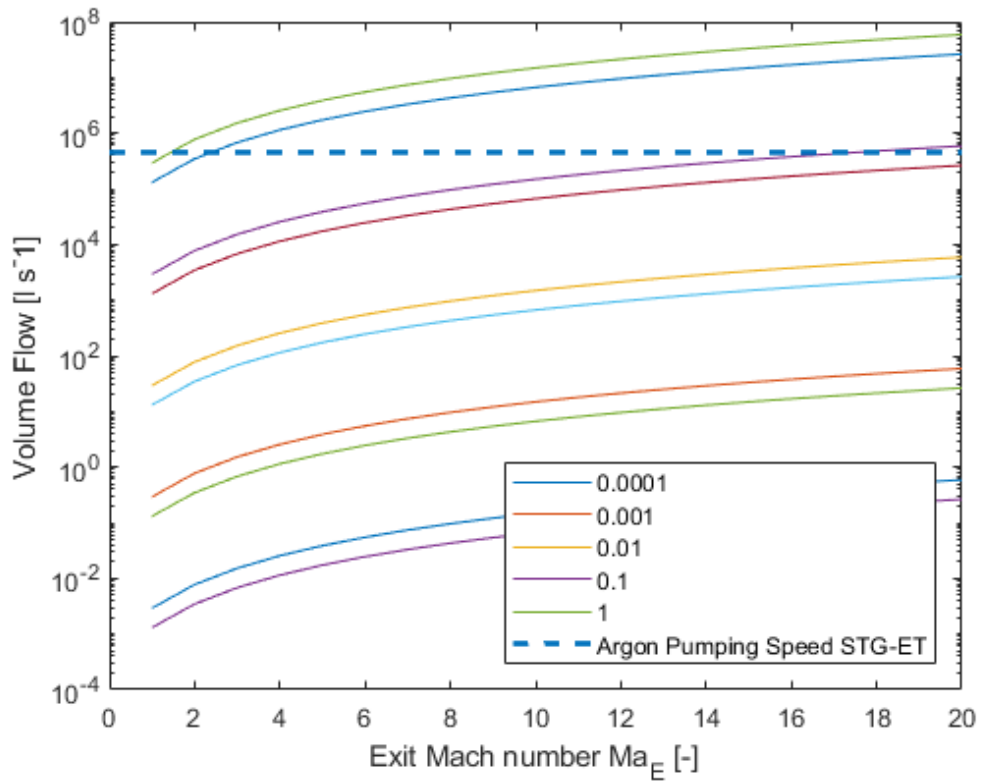
175 The generation of flow conditions similar to the atmosphere at high altitudes is one of the most
176 challenging areas of research. While classic Hypersonic Vacuum Wind Tunnels can be used,
177 they are often limited in experimental time, maximum velocity or densities, since they are
178 optimized for specific points within the trajectory of a spacecraft. A similar requirement goes
179 for the simulation of the VLEO, which requires high velocity ($v_\infty \approx 8 \frac{km}{s}$; $Ma_\infty \approx 13$) at very
180 low pressures ($p = 9 \cdot 10^{-7} - 4 \cdot 10^{-9}$ mbar). While the low pressures are possible within
181 some facilities, such as the V3G, STG-CT, STG-ET, the creation of fast atomic oxygen (FAO)
182 flow is challenging. multiple techniques are possible, which mostly require the creation of a
183 plasma, electrostatic acceleration of ions and neutralization of these [9] similar to the neutral
184 beam injection into nuclear fusion devices. While the necessary beam energies required for the
185 atmospheric flow conditions are lower and therefore require much less power, the necessary
186 setup is still very complex and requires multiple vacuum chambers, high voltage acceleration
187 grids and pumps. Another possibility would be the use of an atomic oxygen beam source as
188 described in [9] working by electron stimulated desorption through an Ag membrane, which
189 could be relatively easily installed within the existing facilities. While this setup requires an
190 electron gun and a heater for the membrane, the dimensions, complexity and required energies
191 are significantly lower compared to neutral beam creation. Finally, the molecular beam
192 technique creating a high velocity flow using Knudsen effusion through an orifice could be
193 implemented within the STG-ET facility. To estimate the feasibility of this option, the design
194 considerations of the V3G wind tunnel [13] are applied to the STG-ET facility. For a continuum
195 flow, the mass flow \dot{m} through the exit of a nozzle with exit area A_E is given by

$$196 \quad \dot{m} = \rho_E u_E A_E = \rho_E u_E \frac{\pi}{4} D_E^2$$

197 in which ρ_E is the density at the nozzle exit. For the exit velocity u_E and Mach number Ma_E ,
 198 the relation $u_E = Ma_E \sqrt{\kappa R T_E}$, in which $T_E = T_0 (1 + \frac{\kappa-1}{2} Ma_E^2)^{-1}$ is the temperature at the
 199 nozzle exit in relation to the reservoir temperature T_0 , can be used to find a relation between
 200 vacuum pump volume flow, exit Mach number and nozzle diameter

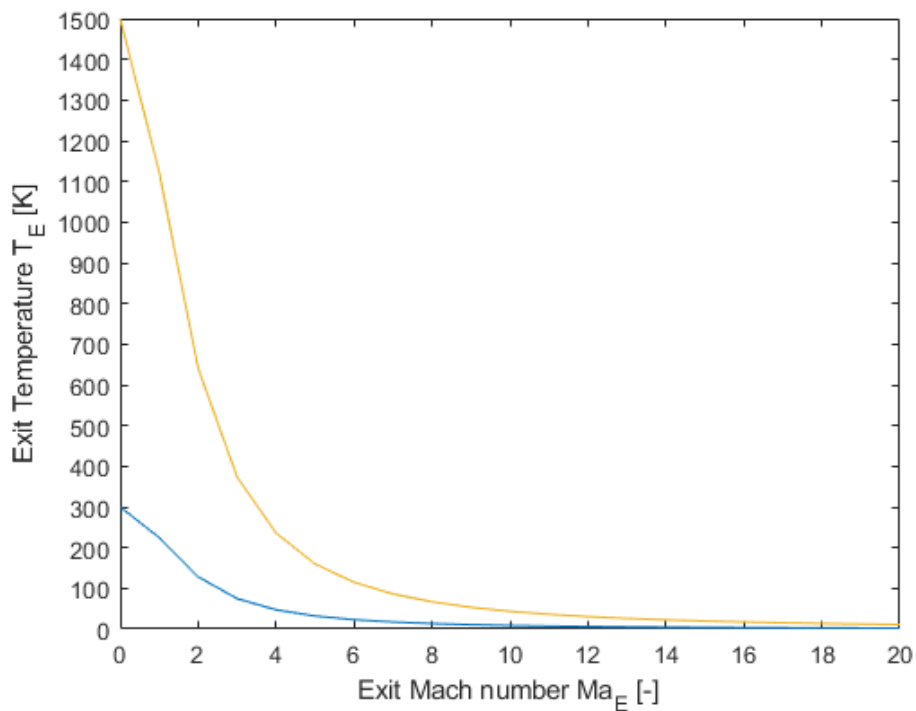
$$201 \quad \dot{V} = \frac{\pi}{4} \sqrt{\kappa R} \frac{T_p}{\sqrt{T_0}} Ma_E \sqrt{1 + \frac{\kappa-1}{2} Ma_E^2} \frac{p_E}{p_p} D_E^2$$

202 using the relation for the mass flow of a pump $\dot{m} = \frac{p_p \dot{V}}{R T_p}$ in which p_p and T_p are the pressure and
 203 temperature at the pump. While in reality, the pressure and temperature distribution within the
 204 STG-ET is more complex, especially considering cryopumps, for this simplified analysis we
 205 assume that the vacuum pressure is equal to the pressure at the pumps $p_E = p_p$. Initially, we
 206 will also assume that the temperature at the pump and the reservoir temperature are equal,
 207 leading to $T_p = T_0$.



208

209 *Figure 9: Required pumping volume flow as a function of nozzle exit Mach Number for*
 210 *reservoir temperature of 300K and 1500K for different nozzle exit diameters*



211

212 *Figure 10: Nozzle exit temperature as a function of nozzle exit Mach Number for reservoir*
 213 *temperature of 300K and 1500K*

214 As it can be seen in Figure 9, in which the necessary pumping volume flow are shown as a
 215 function of exit Mach number, for Argon (for which the pumping speed is known) the possible
 216 exit Mach numbers can be very high. Unfortunately, as displayed within Figure 10, due to the
 217 decrease of temperature during the expansion and the following onset of condensation of the
 218 gas, for a reservoir at room temperature a Mach number above 2 is not viable. Even for a heated
 219 reservoir similar to the V2G facility or using an inductive plasma heater, the gas will condensate
 220 for exit Mach numbers above 6. Additionally, the boundary layer within the nozzle will grow
 221 significantly, influencing the center flow. The expansion within an ideal nozzle is not viable for
 222 the creation of high velocity flows within the STG-ET facility. Therefore, it is necessary to use
 223 a freely expanding jet to generate such a high speed flow. In a free jet, the Mach number along
 224 the center line is a function of axial distance x from an orifice with a diameter d [21], [22] given
 225 by

$$226 \quad Ma(x) = A \cdot \left(\frac{x - x_0}{d}\right)^{\kappa-1} \cdot \left(1 - \frac{1}{2} \frac{\kappa + 1}{\kappa - 1}\right)$$

227 for which the constants are given in Table 2, calculated using the method of characteristics. The
 228 distribution of the density along different stream lines is given by

$$229 \quad \frac{\rho(\Theta', x)}{\rho_0} = B \cos^2\left(\frac{\pi\Theta'}{2\phi}\right) \left(\frac{R}{d/2}\right)^{-2}$$

230 *Table 2: Constants of the free jet for different adiabatic coefficients*

κ	$\frac{x_0}{d}$	A	ϕ	B
1.67	0.075	3.26	1.365	0.643
1.4	0.4	3.65	1.665	0.357
1.2857	0.85	3.96	1.888	0.246

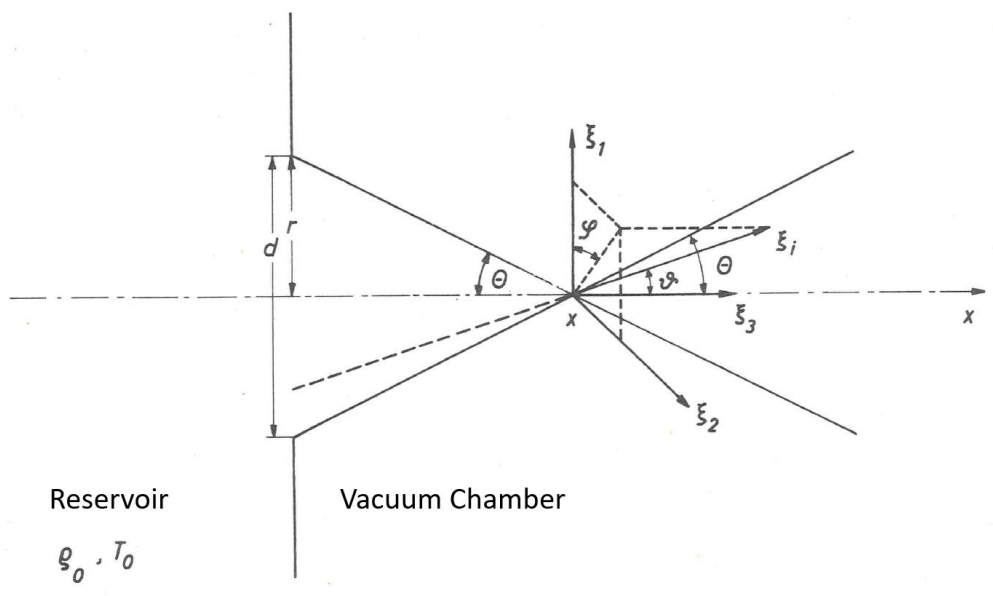
231 For the limiting case of $\frac{\lambda}{d} \gg 1$, when the pressure and density in the reservoir is lowered, the
 232 transition to the Knudsen effusion as displayed in Figure 11 begins. Within the reservoir, a
 233 Maxwell distribution of the velocities is assumed and within the vacuum chamber, absolute

234 vacuum is assumed. The distribution function of the particle velocity components ξ_r in polar
 235 coordinates can now be written as

236
$$f_r = \frac{n_0}{(2\pi RT_0)^{3/2}} \cdot \exp\left(\frac{\xi_r^2}{2RT_0}\right)$$

237 And the moment on the axis of the Knudsen effusion becomes

238
$$\langle \phi(\xi_i) \rangle = \int_{\varphi=0}^{2\pi} \int_{\vartheta=0}^{\theta} \int_{\xi_r=0}^{\infty} \phi(\xi_i) f_r \xi_r^2 \sin\vartheta d\varphi d\vartheta d\xi_r$$



239
 240 *Figure 11: Scheme and variables of the Knudsen effusion through an orifice with diameter d*

241 The values of the flow along the stream can now be written as a function of the angle θ , which

242 can also be written as $\theta = \text{arc tg } \frac{r}{x}$. The variables of the flow now become $n = n_0 \sin^2 \frac{\theta}{2}$ for

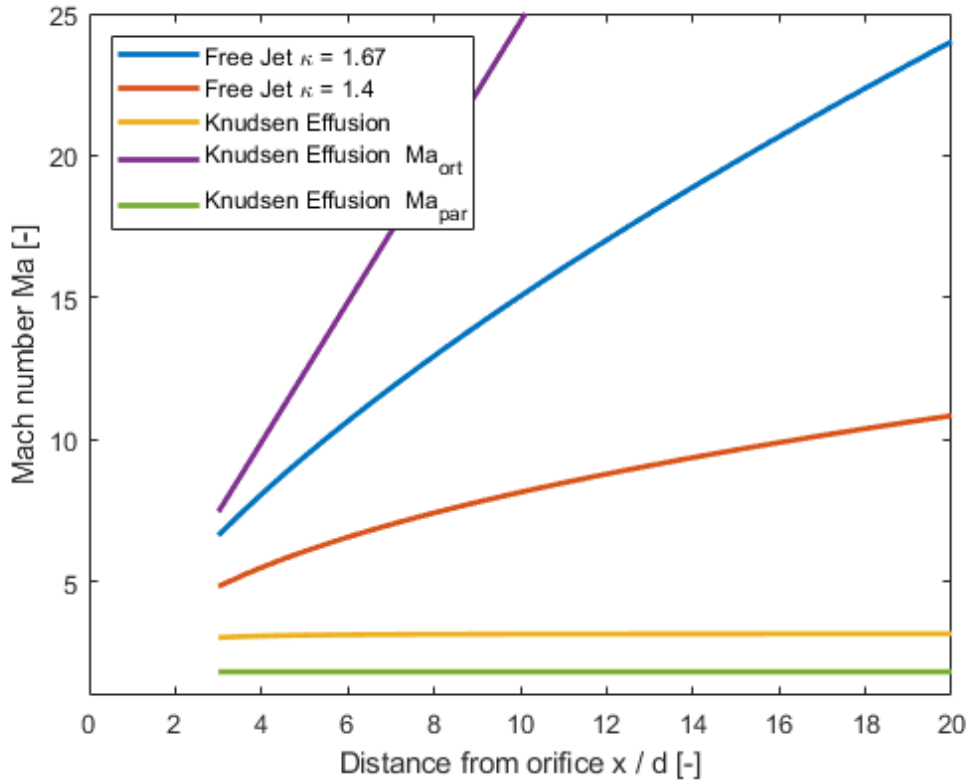
243 the number density, $u_i = \frac{2\sqrt{2RT_0}}{\sqrt{\pi}} \{0, 0, \cos^2 \frac{\theta}{2}\}$ for the flow velocity and $T = T_0 \left(1 - \frac{8}{3\pi} \cos^4 \frac{\theta}{2}\right)$

244 for the temperature. We can now gain the value for the ratio of molecular speed

246
$$S = \frac{U}{\sqrt{2RT}} = \frac{2}{\sqrt{\pi}} \frac{\cos^2 \frac{\theta}{2}}{\sqrt{\left(1 - \frac{8}{3\pi} \cos^4 \frac{\theta}{2}\right)}} = Ma \sqrt{\frac{\kappa}{2}}$$

245 .

247 Therefore, in Figure 12 we can now display the axial distribution of the Mach number a freely
 248 expanding jet for the flow within continuum and also for the limit of free molecular flow.



249

250 *Figure 12: Axial Mach number of a free jet within a continuum flow and parallel and*
 251 *orthogonal Mach number for the limit of Knudsen effusion as a function of dimensionless*
 252 *distance x/d from the orifice*

253 As we can see, within a free jet, very high Mach numbers of up to 20 for Argon or 13 for
 254 nitrogen can be reached. The position of the compression shock at the end of the free jet can be

255 found from $\frac{x_M}{d} = 0.67 \left(\frac{p_0}{p_p} \right)^{1/2}$ with the chamber pressure p_p . This ratio is independent of

256 adiabatic coefficient, condensation or nozzle geometry. Since in the STG-ET due to its high

257 pumping capacity and very low pressures, a high ratio of $\frac{p_0}{p_p} > 1000$ can be assumed even if

258 the reservoir is just at atmospheric pressure, $\frac{x_M}{d} \approx 21$, therefore a very high Mach number can

259 be reached just by the expansion of a free jet into the vacuum of the chamber. This is again

260 limited by partial condensation of the gas and the limit in which for the density of the free jet

261 becomes so low which is comparable to the background pressure of the vacuum chamber.

262 **6. Conclusions**

263 A brief overview of the different vacuum chambers and wind tunnels at DLR Göttingen has
264 been given to demonstrate their capabilities to simulate the VLEO. It has been found, that in
265 terms of pressures and pumping capacity, the V3G vacuum wind tunnel and the STG-ET
266 vacuum chamber are the most viable options to create such a facility. These facilities also have
267 rather large dimensions, making it possible to also test larger types of equipment and neglect
268 the influence of reflections from the chamber walls. The analysis of the viability has been done
269 by employing the calculation methods for a free jet used for the design of the V3G wind tunnel
270 on the parameters STG-ET facility. It has been found that very high Mach numbers can be
271 reached by expanding a (molecular) free jet through an orifice until the limit of Knudsen
272 expansion. Other techniques to achieve high velocity flow of neutrals, such as an atomic oxygen
273 source or neutral beam injection using the acceleration of a plasma are also viable but require
274 further study of these technologies. Additionally, the pumping capacity of the STG-ET facility
275 has been tested with noble gases only, and a measurement of the pumping speed for air, nitrogen
276 and oxygen is necessary to further understand the feasibility of the facility for the simulation of
277 the VLEO or other orbital environments. Based on these analyses, a more detailed design of a
278 VLEO wind tunnel can be obtained in the future.

279 **References**

- 280 [1] N. H. Crisp *et al.*, “The benefits of very low earth orbit for earth observation missions,”
281 *Prog. Aerosp. Sci.*, vol. 117, p. 100619, Aug. 2020, doi:
282 10.1016/j.paerosci.2020.100619.
- 283 [2] C. Traub *et al.*, “On the exploitation of differential aerodynamic lift and drag as a means
284 to control satellite formation flight,” *CEAS Space J.*, vol. 12, no. 1, pp. 15–32, Jan. 2020,
285 doi: 10.1007/s12567-019-00254-y.
- 286 [3] F. Romano, B. Massuti-Ballester, T. Binder, G. Herdrich, S. Fasoulas, and T. Schönherr,
287 “System analysis and test-bed for an atmosphere-breathing electric propulsion system
288 using an inductive plasma thruster,” *Acta Astronaut.*, vol. 147, pp. 114–126, Jun. 2018,
289 doi: 10.1016/j.actaastro.2018.03.031.
- 290 [4] C. M. Kelly and J. M. Little, “Performance Scaling and Mission Applications of Drag-
291 Modulated Plasma Aerocapture,” presented at the The 36th International Electric
292 Propulsion Conference, Vienna, Austria, Sep. 2019.
- 293 [5] D. Gonzales *et al.*, “Modelling and Simulation of Very Low Earth Orbits,” p. 10 pages,
294 2019, doi: 10.13009/EUCASS2019-176.
- 295 [6] V. Oiko *et al.*, “Ground-Based Experimental Facility for Orbital Aerodynamics
296 Research: Design, Construction and Characterization,” presented at the 71st
297 International Astronautical Congress (IAC), The Cyberspace, Oct. 2020.
- 298 [7] A. H. Stambler, K. E. Inoshita, L. M. Roberts, C. E. Barbagallo, K. K. de Groh, and B.
299 A. Banks, “Ground-Laboratory to In-Space Atomic Oxygen Correlation for the PEACE
300 Polymers,” *AIP Conf. Proc.*, vol. 1087, no. 1, pp. 51–66, Jan. 2009, doi:
301 10.1063/1.3076865.

- 302 [8] J. Kleiman, S. Horodetsky, and V. Issouпов, “Concept of a New Multifunctional Space
303 Simulator for Accelerated Ground-based Testing in Modern Space Exploration Era,”
304 *AIP Conf. Proc.*, vol. 1087, no. 1, pp. 432–452, Jan. 2009, doi: 10.1063/1.3076857.
- 305 [9] J. Kleiman, Z. Iskanderova, Y. Gudimenko, and S. Horodetsky, “Atomic oxygen beam
306 sources: a critical overview,” vol. 540, pp. 313–324, Sep. 2003.
- 307 [10] J. M. Picone, A. E. Hedin, D. P. Drob, and A. C. Aikin, “NRLMSISE-00 empirical
308 model of the atmosphere: Statistical comparisons and scientific issues,” *J. Geophys. Res.*
309 *Space Phys.*, vol. 107, no. A12, p. SIA 15-1-SIA 15-16, 2002, doi:
310 <https://doi.org/10.1029/2002JA009430>.
- 311 [11] G. Koppenwallner, “The hypersonic low density wind-tunnel of the Aerodynamische
312 Versuchsanstalt Goettingen - Operational behaviour and results on vibrational
313 relaxation,” in *6th Aerospace Sciences Meeting*, 0 vols., American Institute of
314 Aeronautics and Astronautics, 1968. doi: 10.2514/6.1968-49.
- 315 [12] W. Wuest, G. Koppenwallner, G. Hefer, and H. Legge, “Der Hypersonische
316 Vakuumwindkanal der aerodynamischen Versuchsanstalt Göttingen,” *Jahrb. DGLR*, pp.
317 38–51, 1969.
- 318 [13] H. Legge, “Entwurfsgrundlagen und kurze Baubeschreibung der dritten Meßstrecke des
319 Hypersonischen Windkanals für kleine Gasdichten der DFVLR-AVA in Göttingen,”
320 DFVLR, Göttingen, Forschungsbericht 71–84, 1971.
- 321 [14] A. Neumann, “STG-ET: DLR electric propulsion test facility,” *J. Large-Scale Res.*
322 *Facil. JLSRF*, vol. 3, no. 0, Art. no. 0, Apr. 2017, doi: 10.17815/jlsrf-3-156.
- 323 [15] A. Neumann, “STG-ET: DLR Electric Propulsion Test Facility,” *J. Large-Scale Res.*
324 *Facil. JLSRF*, vol. 4, no. 0, Art. no. 0, Nov. 2018, doi: 10.17815/jlsrf-3-156-1.
- 325 [16] M. Grabe, “STG-CT: High-vacuum plume test facility for chemical thrusters,” *J. Large-*
326 *Scale Res. Facil. JLSRF*, vol. 2, no. 0, Art. no. 0, Aug. 2016, doi: 10.17815/jlsrf-2-139.

- 327 [17] T. Schlegat, “Experimental investigation of rarefaction effects on aerodynamic
328 coefficients of slender and blunt re-entry vehicles,” Thesis.Doctoral. Accessed: Jun. 07,
329 2021. [Online]. Available: [http://geb.uni-](http://geb.uni-giessen.de/geb/frontdoor.php?source_opus=13561&la=de)
330 [giessen.de/geb/frontdoor.php?source_opus=13561&la=de](http://geb.uni-giessen.de/geb/frontdoor.php?source_opus=13561&la=de)
- 331 [18] H. Müller, “Über die Erzeugung hoher Ruhetemperaturen für molekulare hypersonische
332 Strömungen mittels eines Induktions-Plasma-Brenners,” DFVLR, Göttingen, Interner
333 Bericht 063-72 H 14, 1972.
- 334 [19] L. J. Buntrock, C. Volkmar, and K. Hannemann, “Sputtering of Mo and Ag with xenon
335 ions from a radio-frequency ion thruster,” *Rev. Sci. Instrum.*, vol. 92, no. 4, p. 045109,
336 Apr. 2021, doi: 10.1063/5.0031408.
- 337 [20] A. Neumann, K. Hannemann, and M. Brchnelova, “Challenges of Cryopumping EP-
338 Propellants in DLR’s Electric Propulsion Test Facility,” presented at the The 36th
339 International Electric Propulsion Conference, Vienna, Austria, Sep. 2019.
- 340 [21] H. Legge, “Kraft- und Wärmeübergang in freier Molekülströmung mit verschiedenen
341 Verteilungsfunktionen von Expansionsströmungen,” *ZAMM - J. Appl. Math. Mech. Z.*
342 *Für Angew. Math. Mech.*, vol. 50, no. 1–4, pp. 193–195, 1970, doi:
343 10.1002/zamm.19700500194.
- 344 [22] H. Ashkenas and F. S. Sherman, “The Structure and Utilization of Supersonic Free Jets
345 in Low Density Wind Tunnels,” p. 84, 1965.

346